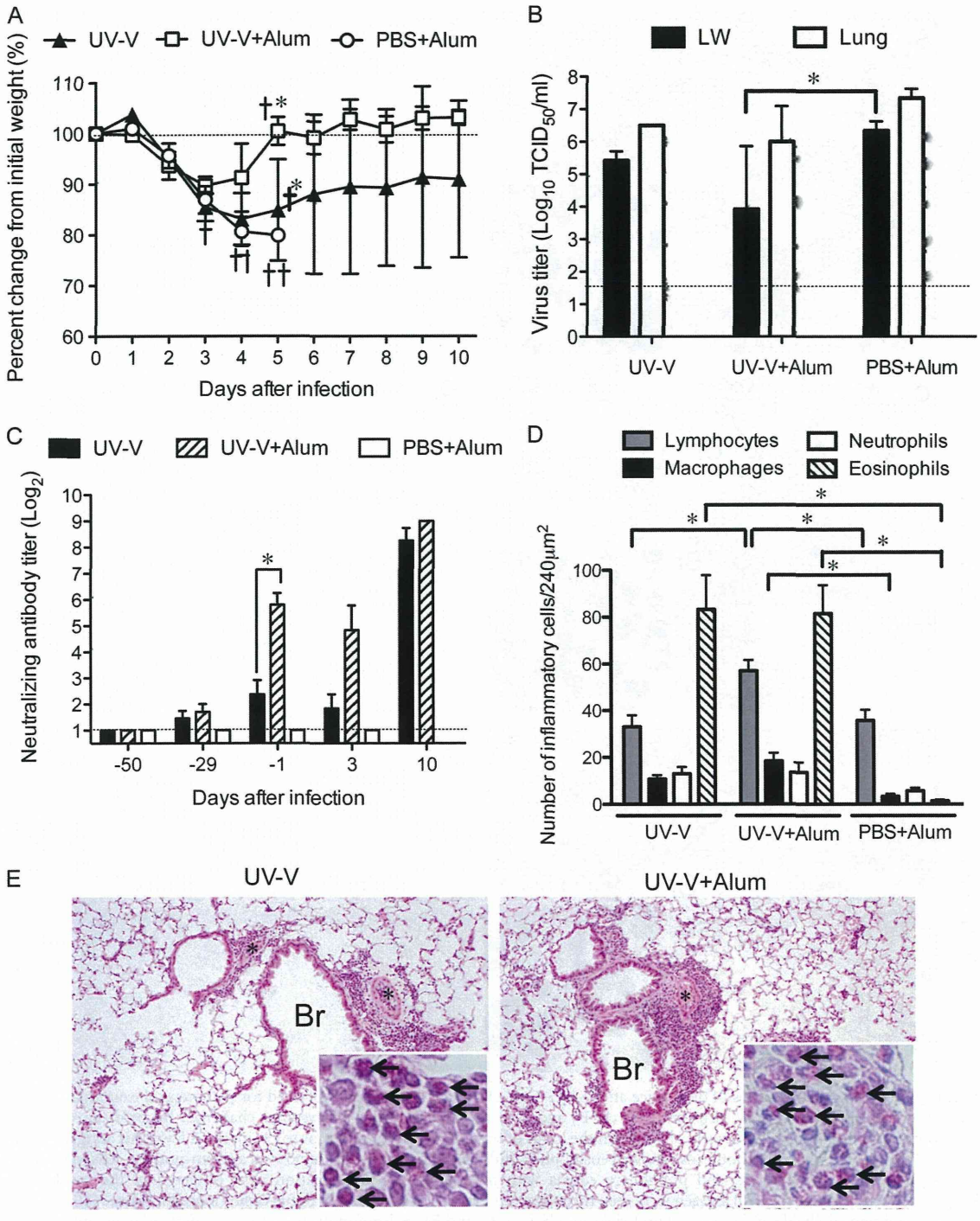

FIG 1 Immunization with UV-V induces eosinophilic immune pathology in adult mice after SARS-CoV challenge. Adult female BALB/c mice were vaccinated with UV-V, UV-V with alum (UV-V+Alum), or vehicle (PBS with Alum, PBS+Alum) and subsequently challenged with 1,000 $TCID_{50}$ of F-musX. (A) Body weight changes following the challenge inoculation ($n = 5$). Dead mice are marked with crosses. Error bars indicate standard deviations. Significant differences ($P < 0.05$, one-way ANOVA) between groups are marked with an asterisk. (B) Virus titers in the lungs and lung wash fluids on day 3 postchallenge ($n = 3$). The dashed line indicates the limit of detection ($10^{1.5}$ $TCID_{50}$/ml). Error bars indicate standard deviation. Significant differences ($P < 0.05$, one-way ANOVA) between groups are marked with an asterisk. LW, lung wash fluid. (C) Neutralizing serum antibody titers against SARS-CoV on days 50, 29, and 1 before challenge ($n = 11$) and on days 3 and 10 after challenge ($n = 5$ to 6). Serum samples were 2-fold serially diluted beginning at 1:2. Error bars indicate standard deviations. Significant differences ($P < 0.05$, one-way ANOVA) between groups are marked with an asterisk. (D) Numbers of lymphocytes, macrophages, neutrophils, and eosinophils in lung sections ($n = 3$) on day 3 after challenge. Five 240-μm^2 regions in the extrabronchioles of lung per mouse were examined at magnification ×40. Asterisks indicate $P < 0.05$ by the Bonferroni test. Error bars indicate standard deviations. (E) Representative images of lung sections from UV-V- and UV+Alum-immunized mice on day 10 postchallenge. Hematoxylin-and-eosin (magnification, ×10) and C.E.M. kit (inset; magnification, ×100) staining were used. Br, bronchi; *, blood vessel.

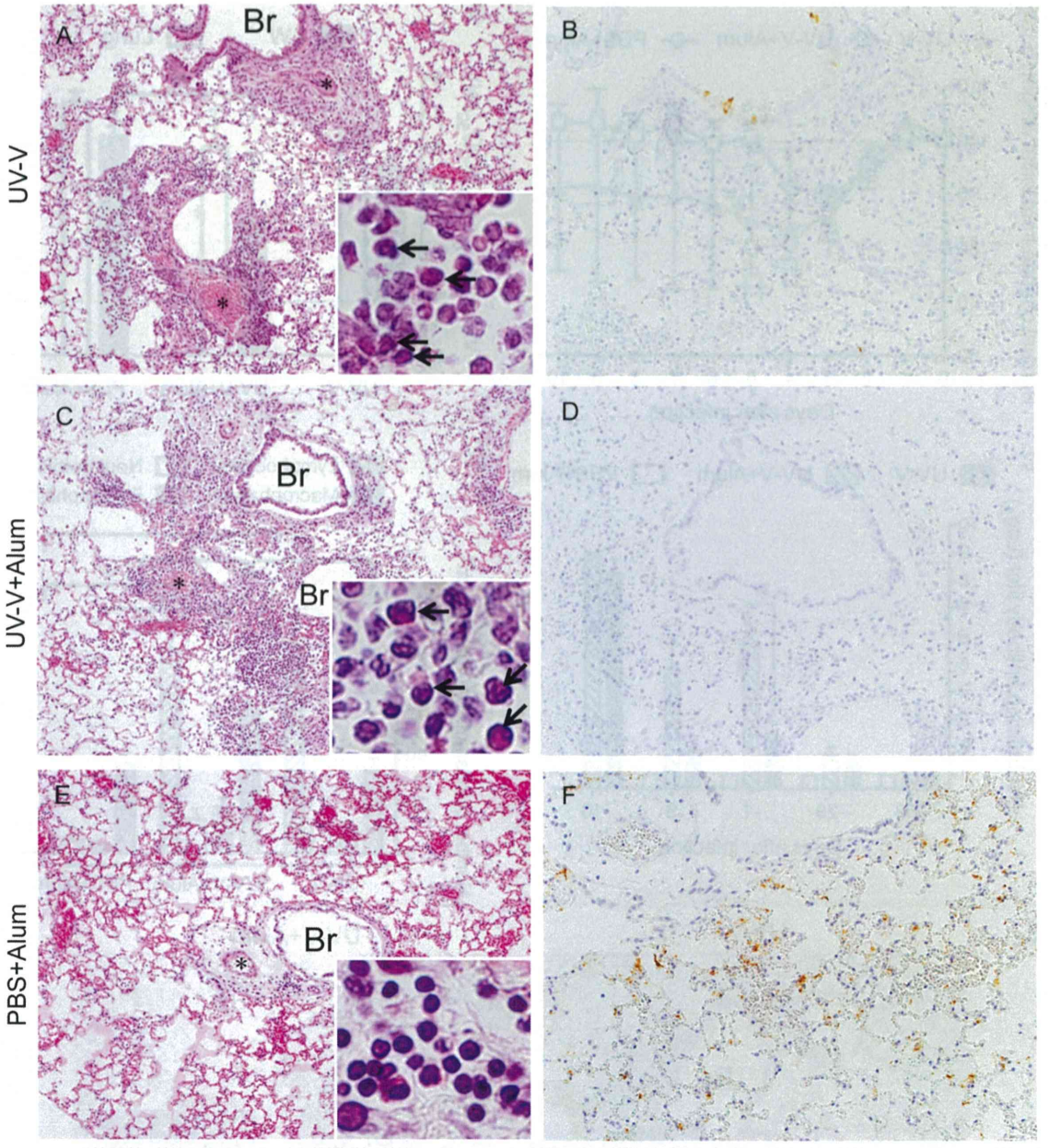

FIG 2 Histopathological findings in the lungs of dead mice after SARS-CoV challenge. Lungs were obtained for pathological examination (A, C, and E) and immunohistochemical analysis of SARS-CoV virus antigens (B, D, and F) from mice that died 5 days after challenge. Br, bronchi; *, blood vessel. Severe inflammatory infiltrates containing eosinophils were observed in the lungs of the UV-V-immunized mouse (A, inset). A few virus antigens were present in the bronchi (B). The UV-V+Alum-immunized mouse also showed eosinophilic inflammatory reactions, but no viral antigen-positive cells were present in the lungs (C, inset, and D). Congestion, hemorrhage, and pulmonary edema with mononuclear cell infiltration were observed in the mock-vaccinated mouse (PBS+Alum) (E, inset). Cells positive for viral antigen were seen throughout the lung (F). Hematoxylin-and-eosin (magnification, ×10) and C.M.E kit (inset; magnification, ×100) staining, a reliable and specific stain for eosinophils (A, C, and E), or immunohistochemical staining with an anti-SARS-CoV antibody (magnification, ×20) (B, D, and F) were used.

differences among UV-V-immunized, UV-V+TLR-immunized, and PBS+Alum-injected mice in the levels of other proinflammatory cytokines and chemokines, including GM-CSF, IFN-γ, IL-12p70, IL-1b, IL-2, IL-5, IL-6, IL-7, MCP-1, MIP-1α, RANTES, and TNF-α. These results indicate that TLR agonists are potent adjuvants that inhibit the skewing of immune responses toward Th2 responses and block the enhanced eosinophilic infiltration into the lungs that occurs after SARS-CoV infection.

Immunization with UV-V plus TLR agonists induces IFN-β gene expression in the lungs after challenge. Stimulation of TLRs-3,-4, and -7 by TLR agonists induces type I IFNs, with the induction of these type I IFNs being the most immediate antiviral host response to many viral infections (25). To confirm the effect due to poly(I·C) injection before challenge in UV-V+TLR-immunized mice, we employed quantitative real-time RT-PCR to assess mRNA expression levels in UV-V- and UV-V+TLR-immunized mice ($n = 6$) 1 day after challenge. The amount of IFN-α4

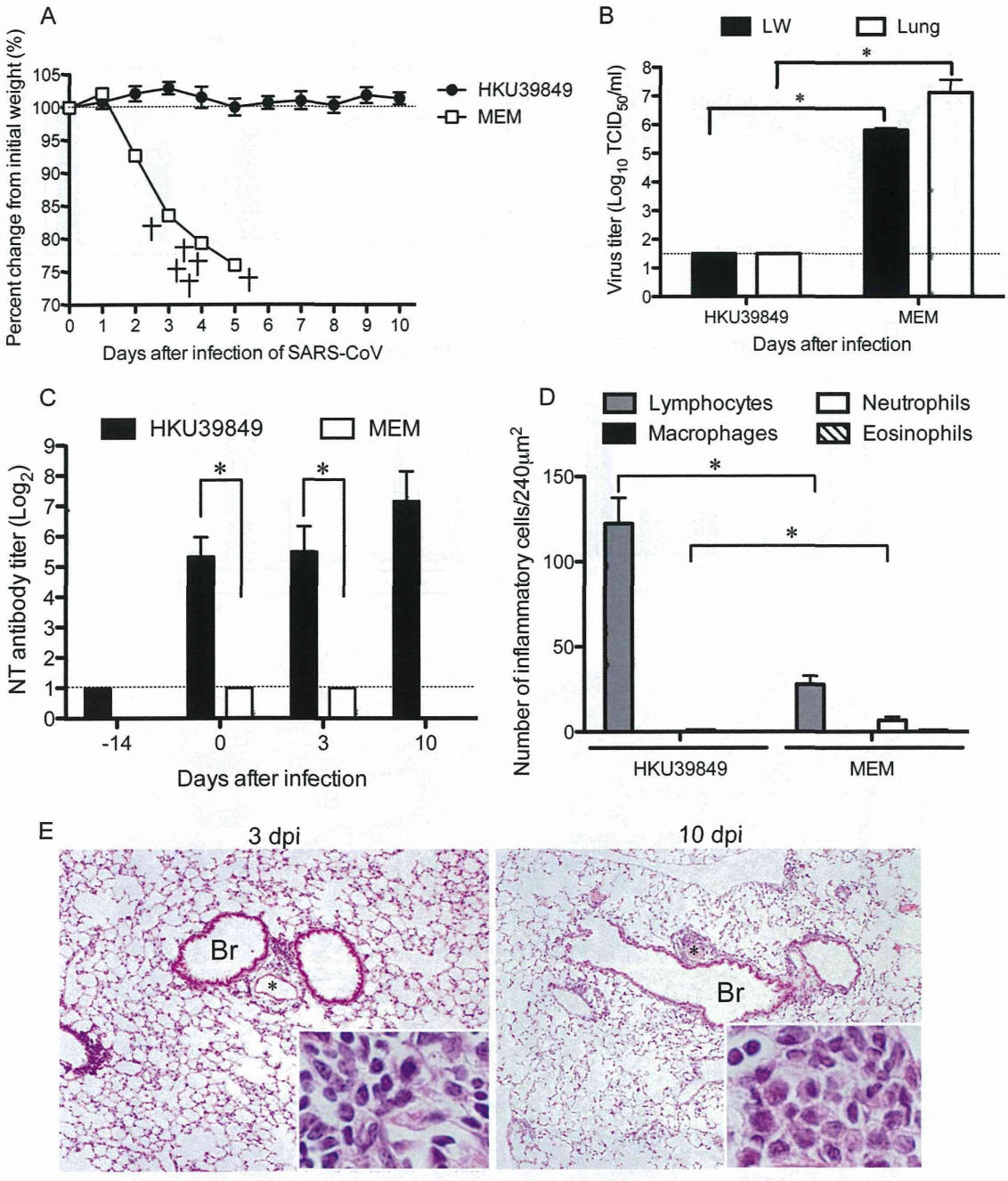

FIG 3 Reinfection with SARS-CoV in aged mice. Aged mice were infected with the HKU39849 isolate or mock vaccinated (no vaccination) and subsequently infected with 1,000 $TCID_{50}$ of F-musX. (A) Mice were weighed daily after challenge. All mock-vaccinated mice died by day 5, but all reinfected mice survived. Dead mice are marked with crosses. Error bars indicate standard deviations. (B) Virus titers in the lungs and lung wash fluids 3 days after challenge ($n = 3$). The dashed line indicates the limit of detection ($10^{1.5}$ $TCID_{50}$/ml). Error bars indicate standard deviations. Significant between-group differences ($P < 0.05$ by one-way ANOVA) are marked with an asterisk. LW, lung wash fluid. (C) Neutralizing serum antibody titers against SARS-CoV on days 0, 3, and 10 after challenge ($n = 6$ to 12). Serum samples were 2-fold serially diluted beginning at 1:2. Error bars indicate standard deviations. Significant between-group differences ($P < 0.05$ by one-way ANOVA) are marked with an asterisk. (D) Numbers of lymphocytes, macrophages, neutrophils, and eosinophils in lung sections ($n = 3$) 3 days after challenge. Five 240-μm^2 regions in the extrabronchioles of each mouse lung were examined at magnification ×40. Asterisks indicate $P < 0.05$ by the Bonferroni test. Error bars indicate standard deviations. (E) Representative images of the lungs of SARS-CoV-reinfected mice. Br, bronchi; *, blood vessel. Lung samples taken 3 and 10 days after infection were sectioned and stained with hematoxylin and eosin (magnification, ×10) and the C.E.M. kit (inset; magnification, ×100).

mRNA did not differ significantly in the lung tissues of UV-V- and UV-V+TLR-immunized mice. Although IFN-β gene expression in the lungs was significantly higher in UV-V+TLR- than in UV-V-immunized mice on day 1 (Fig. 6A), the viral copy number in the lungs of these mice did not differ significantly (Fig. 6B). In addition, ELISAs showed that IFN-α and -β in the sera and lungs of UV-V- and UV-V+TLR- and PBS-infected mice were below the limits of detection 3 and 10 days after challenge.

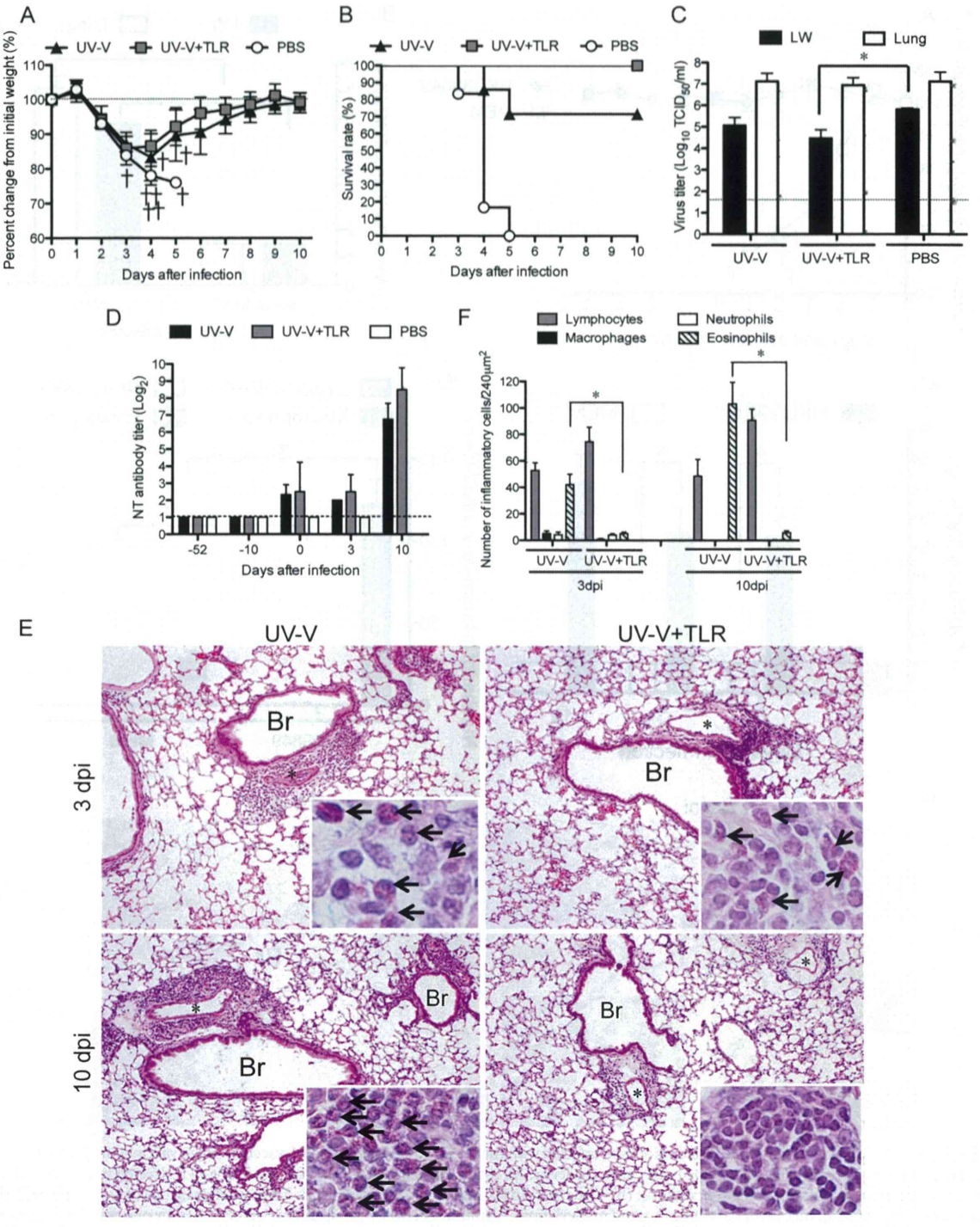

FIG 4 Immunization with UV-V and TLR agonists inhibits excessive eosinophilic infiltration after SARS-CoV challenge. Adult female BALB/c mice were vaccinated with UV-V, UV-V with TLR agonists (UV-V+TLR), or vehicle (PBS) and subsequently challenged with 1,000 $TCID_{50}$ of F-musX. Dead mice are marked with crosses. (A and B) Mice were weighed daily and monitored for morbidity ($n = 6$ to 7). (C) SARS-CoV titers in the lungs and lung wash fluids 3 days after intranasal challenge with SARS-CoV ($n = 4$). Significant differences ($P < 0.05$, one-way ANOVA) between groups are marked with an asterisk. The dashed line indicates the limit of detection ($10^{1.5}$ $TCID_{50}$/ml). Error bars indicate standard deviations. LW, lung wash fluid. (D) SARS-CoV-specific neutralizing serum antibody titers 52, 10, and 0 days before challenge ($n = 13$ to 14) and 3 and 10 days after challenge ($n = 6$ to 7, respectively) with SARS-CoV. Serum samples were 2-fold serially diluted beginning at 1:2. Error bars indicate standard deviations. (E) Representative images of lung sections from mice immunized with UV-V, UV-V+LPS, or UV-V+TLR on days 3 and 10 after challenge with F-musX. Hematoxylin-and-eosin (magnification, ×10) and C.E.M. kit (inset magnification, ×100) staining was used. Br, bronchi; *, blood vessel. (F) Numbers of lymphocytes, macrophages, neutrophils, and eosinophils in the lung sections ($n = 3$). Five 240-μm^2 regions in the extrabronchioles of lung per mouse were examined at magnification ×40. Asterisks indicate $P < 0.05$ by the Bonferroni test. Error bars indicate standard deviations.

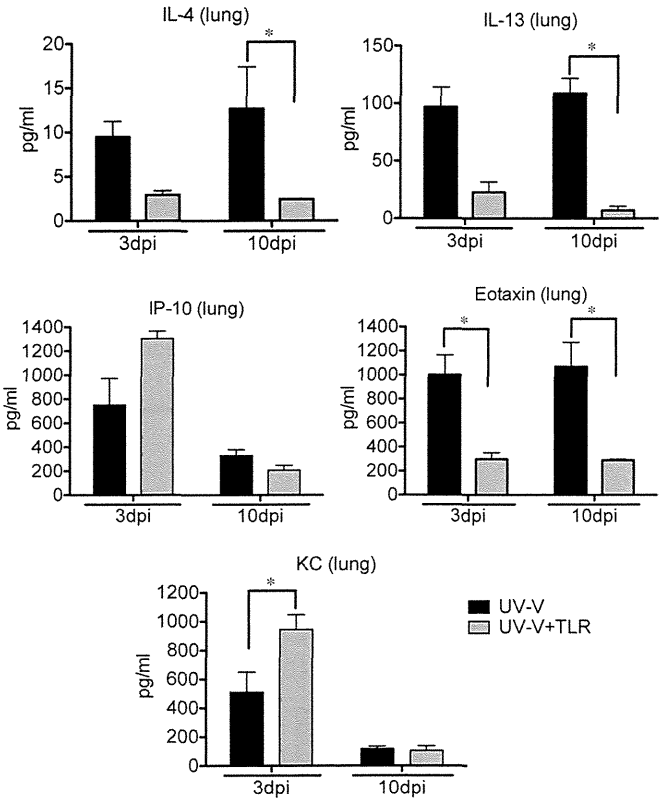

FIG 5 Cytokine and chemokine protein concentrations in lung homogenates of mice immunized with UV-V and challenged with SARS-CoV. The concentrations of cytokines and chemokines in lung homogenates were determined on days 3 and 10 after challenge ($n = 4$). Asterisks indicate significant differences ($P < 0.05$, one-way ANOVA). Error bars indicate standard deviations.

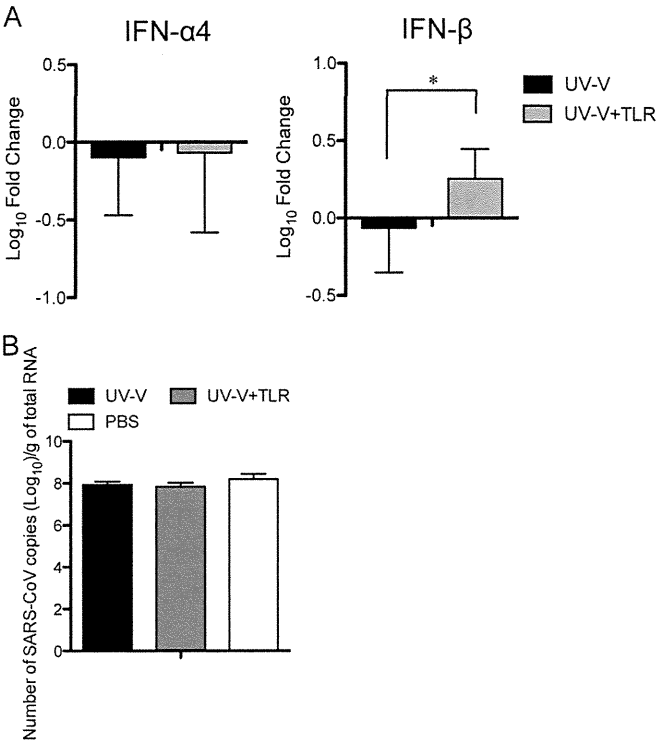

FIG 6 Type I IFN gene expression in lung homogenates of mice immunized with UV-V and challenged with SARS-CoV. Type I IFN mRNA expression profiles in UV-V- and UV-V+TLR-immunized mice (A) or amounts of viral RNA present during infection (B) are shown. RNA was taken from the lungs of UV-V- and UV-V+TLR-immunized mice 1 day after challenge. Type I IFN mRNAs and SARS-CoV genome (nsp11 region) were measured by quantitative real-time RT-PCR. Results are expressed as $\log_{10}$ fold change from results for mock-vaccinated, challenged mice. *, $P < 0.05$. Error bars indicate standard deviations.

Presence of eosinophil infiltration in the lungs after both short- and long-interval UV-V-immunization in response to virus challenge. A second vaccine experiment was performed to evaluate the long-term antiviral efficacy of UV-V+TLR. Fourteen mice per group were immunized with UV-V and UV-V+TLR and boosted 6 weeks later. Four weeks after boosting, the mice were intranasally challenged with F-musX. Both UV-V- and UV-V+TLR-immunized mice showed slight illness and mild loss of body weight but recovered by day 6 (Fig. 7A). Virus titers in the lungs and lung wash fluid on day 3 were below the limit of detection in both UV-V- and UV-V+TLR-immunized mice (Fig. 7B). One day before challenge, the serum titers of neutralizing antibodies were higher in both sets of immunized mice than in the previous experiment, shown in Fig. 4 (Fig. 7C). Microscopic analysis of the lung sections of UV-V-immunized mice 3 days after challenge showed eosinophil infiltration surrounding the bronchi and blood vessels (Fig. 7E), but the number was lower in these mice than in the mice challenged in the experiment shown in Fig. 4 (Fig. 7D). Eosinophil infiltration in the lung was lower on day 10 than on day 3 in UV-immunized mice. After long intervals, the UV-V- and UV-V+TLR-immunized mice seroconverted to produce sufficient neutralizing antibody against SARS-CoV infection. However, both short- and long-interval UV-V-immunization caused eosinophil infiltration in the lungs after challenge.

UV-V-immunized mice showed high expression of genes related to Th2 responses in the lungs after challenge. To better understand the biological pathways by which UV-V-induced pulmonary eosinophilia occurs, we examined global transcriptional changes in mouse lungs. Gene expression profiling was performed using total RNAs from the lungs of mice immunized with UV-V, UV-V+TLR, PBS (as a mock vaccination), or HKU39849 (mimicking live attenuated vaccine) 1 day after F-musX inoculation. A total of 242 genes were differentially regulated between UV-V- and UV-V+TLR-immunized mice. These data are plotted as a heat map, in which each entry represents a gene expression value (Fig. 8A). The data for PBS-injected and HKU39849-inoculated mice were also plotted on a heat map. UV-V- and UV-V+TLR-immunized mice elicited different patterns of gene expression associated with immune responses after SARS-CoV infection. Two trends were observed on the heat maps. Two hundred forty-two genes showed changes in expression level, with 107 genes upregulated and 135 genes downregulated in UV-V-immunized mice. Gene ontology analysis revealed that genes involved in the function, proliferation, differentiation, activation, and maturation of immune cells were expressed similarly, whereas genes associated with chemotaxis, eosinophil migration, eosinophilia, cell movement, and the polarization of Th2 cells were upregulated in UV-V-immunized mice (Table 2; see also Table S1 in the supplemental material) but downregulated in UV-V+TLR-immunized mice. Genes upregulated in UV-V+TLR-immunized mice included those associated with signaling of the proinflammatory cytokines

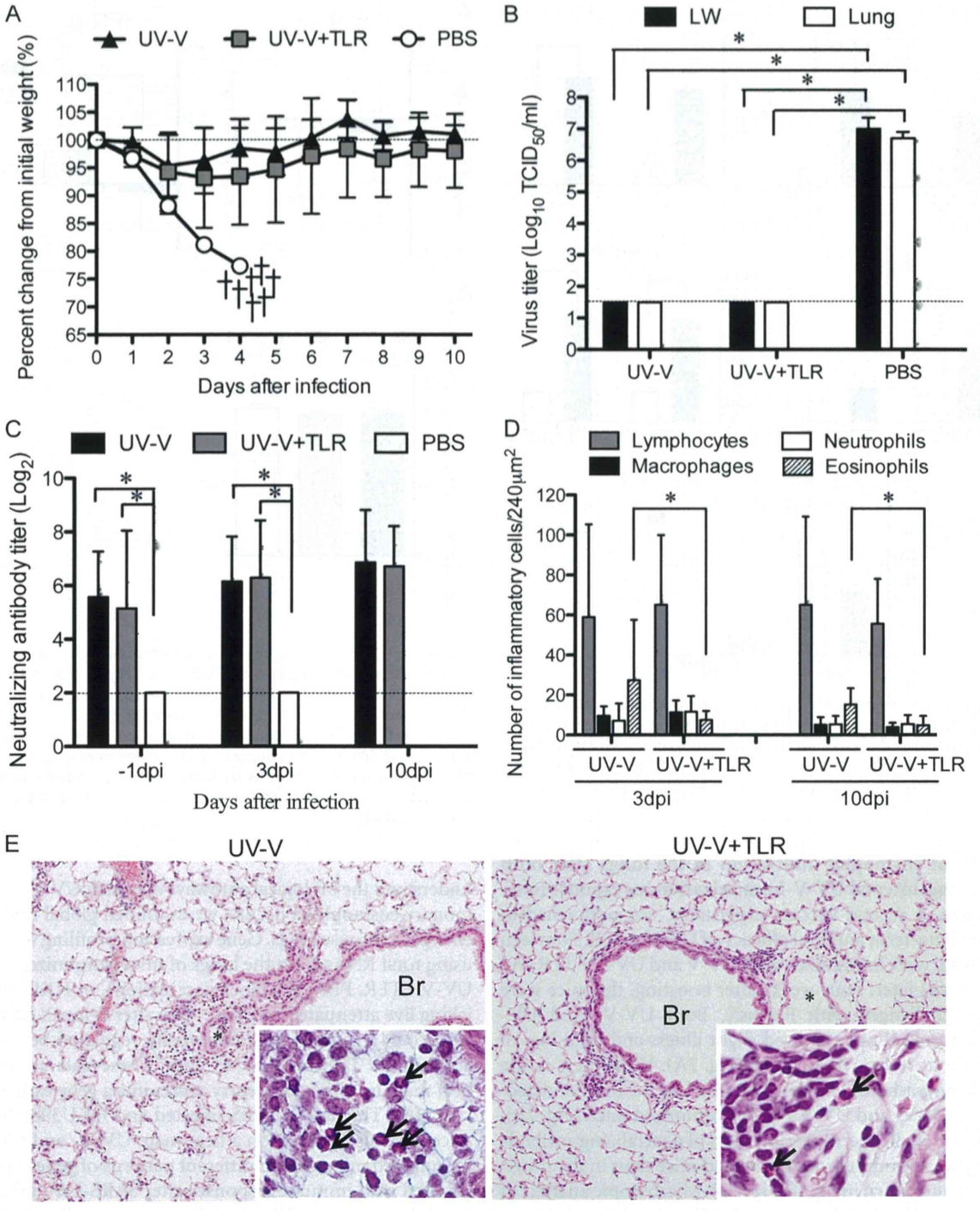

FIG 7 Immunization with UV-V or UV-V+TLR induces eosinophilic immune pathology in adult mice after long-term SARS-CoV challenge. Adult female BALB/c mice were vaccinated with UV-V or UV-V+TLR or mock vaccinated (PBS) and subsequently challenged with 1,000 $TCID_{50}$ of F-musX. (A) Body weight changes following the challenge inoculation ($n = 7$). Dead mice are marked with crosses. Error bars indicate the standard deviations. (B) Titers of virus in the lungs and lung wash fluids on day 3 postchallenge ($n = 4$). The dashed line indicates the limit of detection ($10^{1.5}$ $TCID_{50}$/ml). Error bars indicate standard deviations. Significant between-group differences ($P < 0.05$ by one-way ANOVA) are marked with an asterisk. LW, lung wash fluid. (C) Neutralizing serum antibody titers against SARS-CoV 1 day before challenge ($n = 14$) and 3 and 10 days after challenge ($n = 7$ each). Serum samples were 2-fold serially diluted beginning at 1:2. Error bars indicate standard deviations. Significant between-group differences ($P < 0.05$ by one-way ANOVA) are marked with an asterisk. (D) Numbers of lymphocytes, macrophages, neutrophils, and eosinophils in lung sections ($n = 3$). Five 240-μm^2 regions in the extrabronchioles in the lungs of each mouse were examined at magnification ×40. Asterisks indicate $P < 0.05$ by the Bonferroni test. Error bars indicate standard deviations. (E) Representative images of lung sections from UV-V-immunized (left panel) and UV-V+TLR-immunized (right panel) mice 3 days after challenge. Hematoxylin-and-eosin (magnification, ×10) and C.E.M. kit (inset; magnification, ×100) staining was used. Br, bronchi; *, blood vessel.

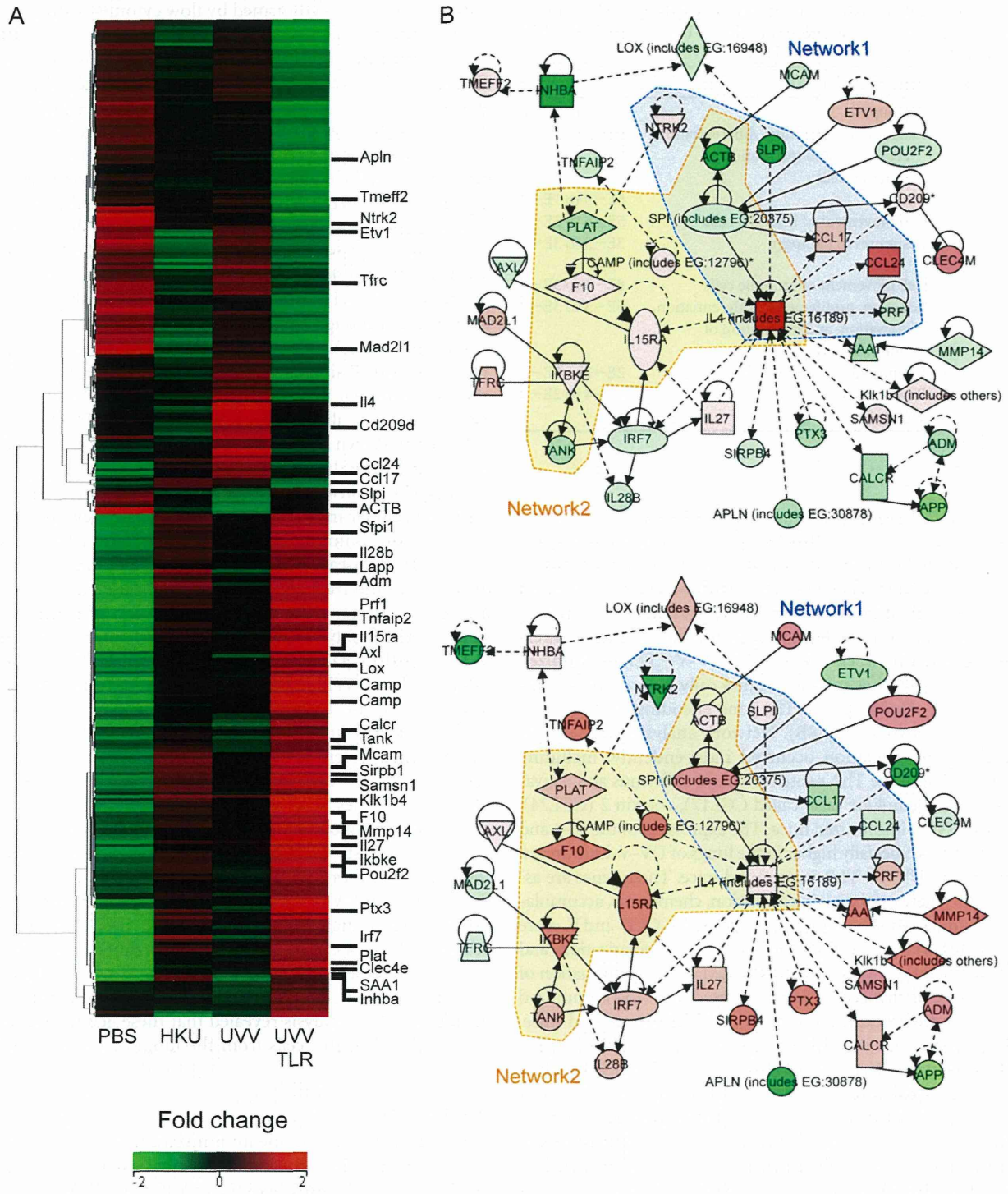

FIG 8 Global gene expression profiles of mice immunized with UV-V after SARS-CoV challenge. An ANOVA was performed to assess differences among all groups. All genes with a greater than 2.0-fold change ($P < 0.05$) in expression, relative to the median of the unchallenged groups, are depicted. Each row represents the lungs of a group of mice ($n = 3$, mock immunization with PBS (PBS); $n = 6$, inoculation with HKU39849 isolate (HKU), UV-V (UVV) or UV-V+TLR (UVVTLR)). The heat map shows the relative levels of expression of 305 probes (242 genes), confirmed statistically by direct comparisons between the UV-V and UV-V+TLR groups. The heat map was generated using the software program GeneSpring GX 12.1. (A) Uncentered Pearson correlation was used as the distance metric with average linkage for unsupervised hierarchical clustering. In the heat map, red represents high expression, black represents median expression, and green represents low expression. The color scale bar at the bottom indicates the relative level of expression. The sidebar on the right indicates genes that are closely related to each other. (B) A gene interaction network including 39 genes was constructed from 242 genes connected by IPA software. The solid and dotted lines indicate direct and indirect interactions, respectively. Genes shown in red were upregulated, and those shown in green were downregulated, compared with the PBS group. The central node is IL-4, a key cytokine in inflammation associated with eosinophils. Network 1 was composed of genes associated with eosinophilia. Network 2 was composed of genes associated with "inflammation of the lungs." The same network is shown for UV-V-immunized (upper panel) and UV-V+TLR-immunized (lower panel) mice.

TABLE 2 Top 5 biological function categories as determined by using IPA for early responses of mice immunized with UV-V and UV-V+TLR and subsequently challenged with SARS-CoV

Immunization	Function annotation	*P* value
UV-V	Eosinophil	7E−5 to 2E−2
	Function, proliferation, differentiation, activation, and maturation of immune cells	6E−5 to 3E−2
	Th2	6E−5 to 1E−2
	Cell movement of immune cells	5E−5 to 3E−2
	Responses to pathogen	3E−5 to 3E−2
UV-V+TLR	Cell movement of immune cells	8E−6 to 3E−3
	Function, proliferation, differentiation, activation, and maturation of immune cells	6E−5 to 3E−2
	Eosinophil	2E−2 to 1E−2
	Responses to pathogen	1E−4 to 2E−2
	Th2	NS[a]

[a] NS, not significant.

TNF-α1 and -2, both of which are regulated by TLRs, including TLR3 and TLR4 (Fig. 9). To assess the interconnection between genes during the host response to virus infection after UV-V immunization, a functional analysis approach was used to construct a graphic network of biologically related genes derived from IPA. This network was constructed by including the 242 genes differentially regulated between UV-V- and UV-V+TLR-immunized mice. Interestingly, this analysis yielded only one network, consisting of 39 of the 242 genes. The gene encoding IL-4 is at the center of this network (Fig. 8B). Network analysis revealed that differential gene regulation occurred independently, including the upregulation of the Th2-related chemokine thymus and activation-regulated chemokine (also called CCL17), eotaxin 2 (CCL24), and IL-4 in UV-V-immunized mice. The expression of the IL-4 and CCL24 genes was especially higher in the lungs of UV-V-immunized than in those of UV-V+TLR-immunized mice. These genes are associated with a network involving attraction, chemotaxis, accumulation, and stimulation of eosinophils. In addition, CCL17 and IL-4 are also associated with Th2 cell movement, homing, polarization, and arrest of proliferation. Most genes associated with "inflammation of the lungs" were unchanged or downregulated in UV-V-immunized mice compared with expression in UV-V+TLR-immunized mice, including actin, beta (ACTB), cathelicidin antimicrobial peptide (CAMP), coagulation factor X enzyme (F10), inhibitor of kappa light polypeptide gene enhancer in B cells, kinase epsilon (IKBKE), interleukin 15 receptor alpha (IL-15RA), IL-4, plasminogen activator, tissue (PLAT), spleen focus-forming virus proviral integration oncogene (SPI1), and TRAF family member-associated NF-κB activator (TANK) (Fig. 8B). Thus, both mRNA and protein assays for host immune responses revealed that the expression of genes related to Th2 responses, especially IL-4, had a key role in the excess eosinophilic immunopathology observed in the lungs of UV-V-immunized mice after subsequent SARS-CoV infection. Such unwanted side effects could be avoided by adding TLR antagonists as an adjuvant.

CD11b$^+$ cells in the lungs of UV-V-immunized mice show upregulation of genes associated with induction of eosinophils after challenge. In addition, gene expression analysis was analyzed in CD11b$^+$ cells, including macrophages, lymphocytes, and granulocytes, which express TLRs (26, 27). The purity of CD11b$^+$ cell populations was confirmed by flow cytometry after magnetic bead separation and was typically greater than 94% (Fig. 10A and D). Microscopic examination revealed that most of the sorted CD11b$^+$ cells were mononuclear small and large cells, but they also included polynuclear cells (Fig. 10B and E). A comparison of the gene expression profiles of CD11b$^+$ cells from UV-V- and UV-V+TLR-immunized mice showed that a total of 434 genes were differentially regulated. To dissect the temporal behavior of key players involved in TLR signaling in more detail, our data were analyzed using IPA. Upstream regulator analysis showed that certain genes were upstream regulators, including TLR3, TLR4, and poly(I·C) (see Table S2 in the supplemental material). To better understand the relationships of these genes, pathway networks were built. Although many networks could be constructed, we limited our investigation to the networks associated with the TLR3, -4, and -7 signaling pathways in order to understand the effect of treatment with TLR agonists on CD11b$^+$ cells. The network of differentially expressed genes related to TLR3, TLR4, and poly(I·C) is shown in Fig. 10C and F; a network for TLR7 could not be built from these data. The network involving TLR3, TLR4, and poly(I·C) consisted of 37 genes, many of which were associated with cellular movement, hematological system development and function, immune cell trafficking, inflammatory response, and infectious disease. There was no difference in gene expression in UV-V-immunized and UV-V+TLR-immunized mice following mock infection. The levels of expression of genes encoding solute carrier family 5, member 5 (SLC5A5), interferon regulatory factor 1 (IRF1), gamma interferon-induced GTPase (Igtp), immunity-related GTPase family M member 2 (Irgm2), interferon-inducible GTPase 1 (Iigp1), chemokine (C-X-C motif) ligand 9 (CXCL9), CD40, guanylate binding protein 4 (GBP4), and guanylate binding protein 2 (GBP2) were especially higher in CD11b$^+$ cells from UV-V+TLR-immunized than from UV-V-immunized mice. These genes were associated with cellular movement, recruitment of leukocytes, and maturation of antigen-presenting cells. In contrast, CD11b$^+$ cells from UV-V-immunized mice showed much more robust regulation of genes in this network than cells from UV-V+TLR-immunized mice. However, several of these genes, including those encoding CXCL2, plasminogen activator receptor (PLAUR), lactotransferrin (LTF), TNF-inducible gene 6 protein (TNFAIP6), CXCL9, and poly(I·C) RNA, have also been implicated in eosinophil migration and eosinophilia of the airways. IPA analysis revealed that these genes were also upregulated in CD11b$^+$ cells from the lungs of UV-V-immunized mice.

DISCUSSION

This study describes vaccine immunization, both with attenuated live and inactivated vaccines, and virus challenge using adult BALB/c mice and mouse-passaged SARS-CoV. This model is useful in the evaluation of efficacies and side effects of vaccine candidates. Several strategies have been considered for vaccination against SARS-CoV (reviewed in reference 28). Spike protein, but not envelope, membrane, or N proteins, protects vaccinated animals from SARS-CoV infection by inducing neutralizing antibodies (29–31) and strong cellular immunity. Antibodies detected in the sera of patients infected with SARS-CoV were directed against at least eight different proteins and bound to viral membranes (32). These findings indicate that multiple epitopes and proteins may be targets of protective antibodies. Although vaccination

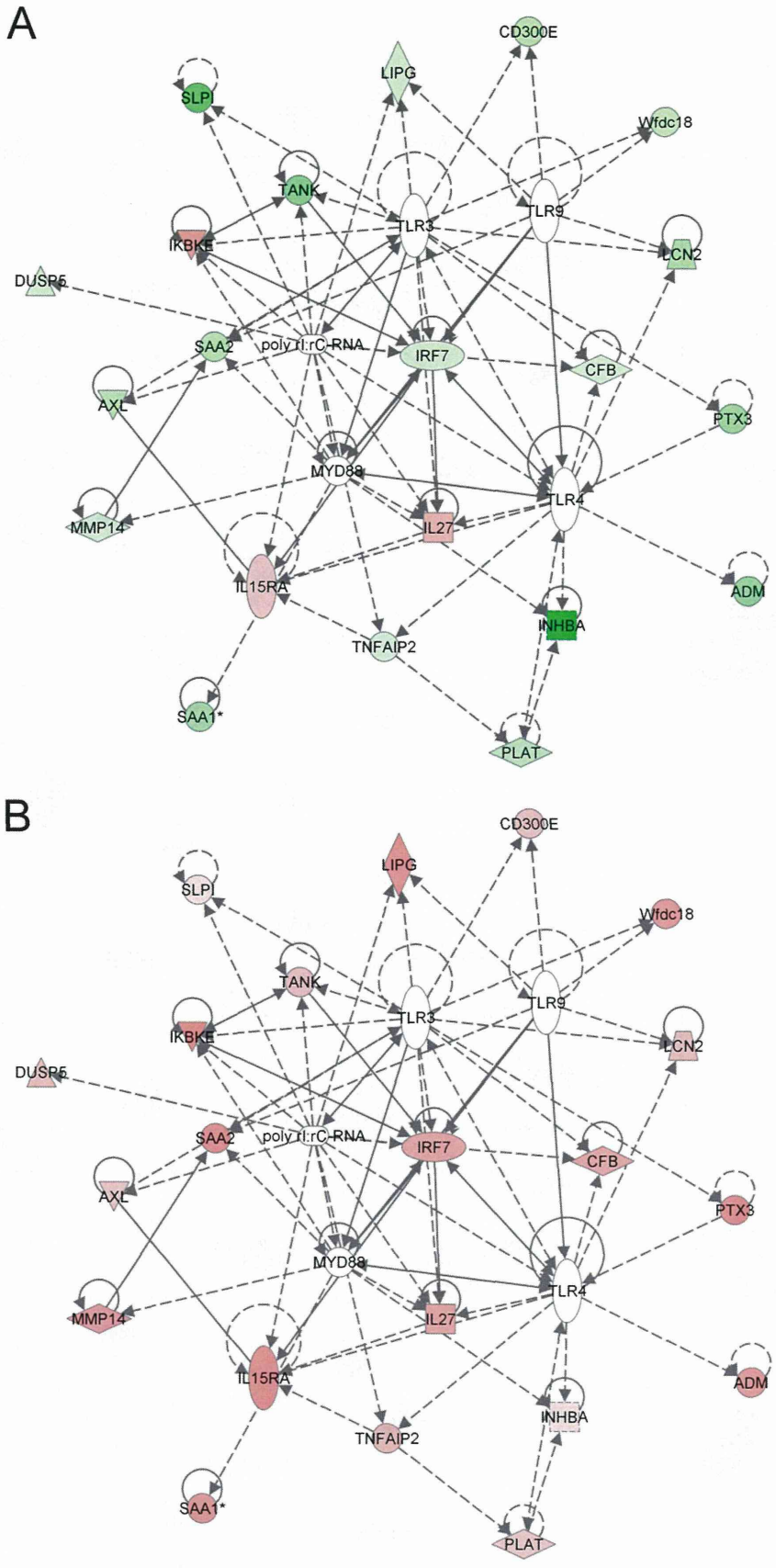

FIG 9 A network of genes in mice immunized with UV-V after SARS-CoV challenge. A direct comparison of gene expression profiles in the lungs of UV-V- and UV-V+TLR-immunized mice is shown. The diagrams show the TLR3 and TLR4 signaling pathways. Genes shown in red were upregulated, and those in green were downregulated, compared with expression for the PBS group. Several genes downstream of TLR3 and TLR4 signaling were upregulated in UV-V+TLR-immunized mice (B) compared with expression in UV-V-immunized mice (A). We overlaid gene expression data on the formed network using Ingenuity Pathway Analysis software.

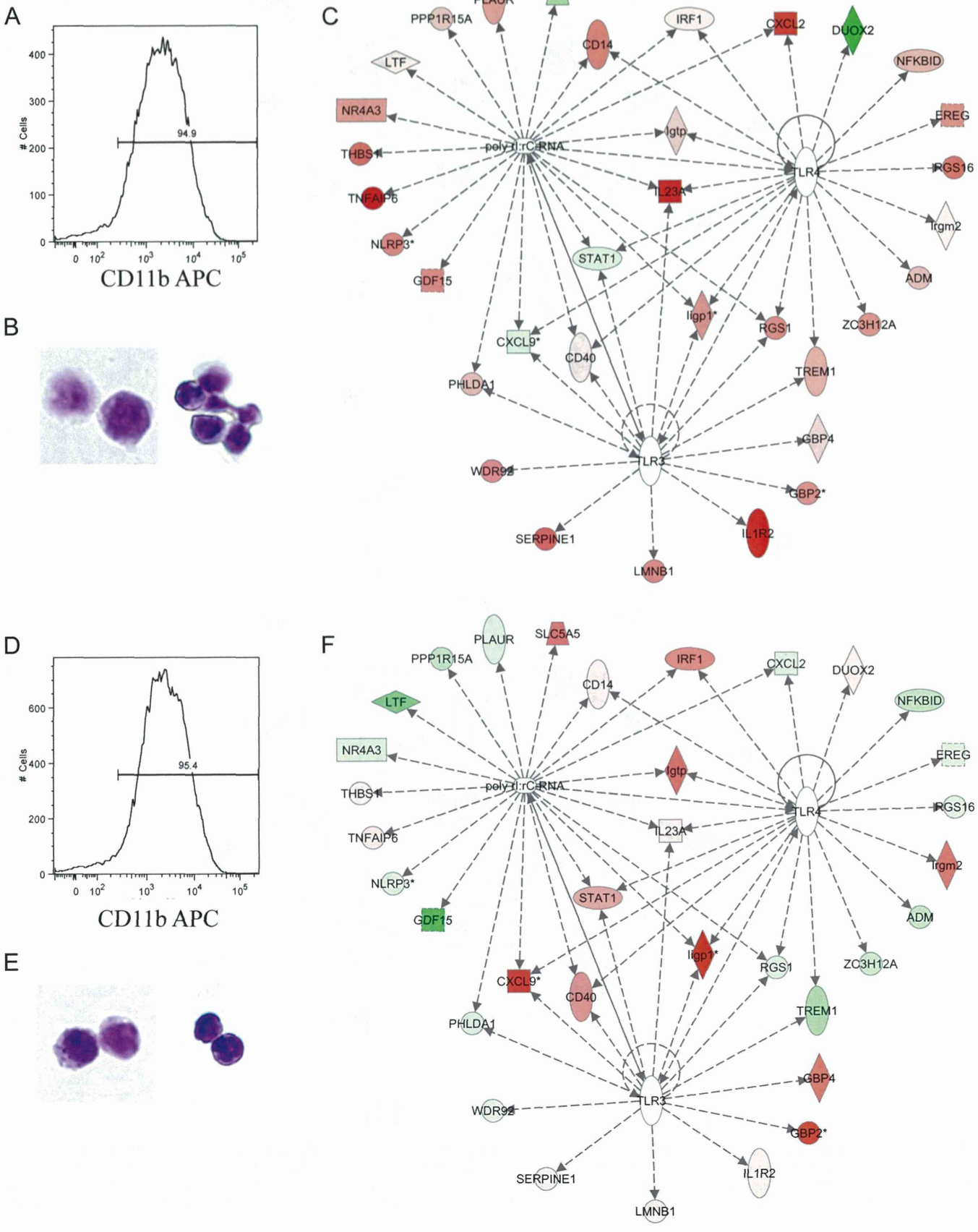
A
Cells
94.9
CD11b APC
B
C
PLAUR
SLC5A5
PPP1R15A
IRF1
CXCL2
DUOX2
CD14
LTF
NFKBID
NR4A3
EREG
Igtp
THBS1
poly I:rC RNA
TLR4
RGS16
TNFAIP6
IL23A
Irgm2
NLRP3*
STAT1
ADM
GDF15
Iigp1*
RGS1
ZC3H12A
CXCL9*
CD40
TREM1
PHLDA1
GBP4
TLR3
WDR92
GBP2*
SERPINE1
IL1R2
LMNB1
D
Cells
95.4
CD11b APC
E
F
PLAUR
SLC5A5
PPP1R15A
IRF1
CXCL2
DUOX2
CD14
LTF
NFKBID
NR4A3
EREG
Igtp
THBS1
poly I:rC RNA
TLR4
RGS16
TNFAIP6
IL23A
Irgm2
NLRP3*
STAT1
ADM
GDF15
Iigp1*
RGS1
ZC3H12A
CXCL9*
CD40
TREM1
PHLDA1
GBP4
TLR3
WDR92
GBP2*
SERPINE1
IL1R2
LMNB1

with attenuated viruses is more efficacious than that with inactivated viruses due to their persistence in the host, attenuated viruses carry the risk of reversion of virulence or recombination repair (33). Due to safety concerns, it is often difficult to gain regulatory approval of attenuated vaccines without strong proof that the threat of disease is sufficient to warrant their use. This threshold has not yet been met for SARS, although some interesting attenuated mutants have been developed (34–36). In contrast, inactivated vaccines do not carry risks of mutating and reverting back to their virulent forms. UV-V virions have been successful due to large-scale production, the presentation of multiple epitopes, and the generation of high levels of humoral immunity in young BALB/c mice injected subcutaneously (37). However, SARS-CoV challenge has not been tested in more vulnerable animals.

In this study, we successfully evaluated the efficacy of UV-inactivated whole-virion immunization in a lethal adult mouse model of SARS-CoV infection. Adult BALB/c mice immunized with UV-V failed to inhibit viral infection and replication within the lungs on day 3. This was one cause of death after subsequent SARS-CoV infection and of enhanced lung immunopathology characterized by increased infiltration by eosinophils. These findings are consistent with studies of vaccine formulations incorporating SARS-CoV N protein and also SARS-CoV doubly inactivated with formalin and UV irradiation (11–14). An excessive host immune response against the N protein of SARS-CoV enhances eosinophilic infiltration into the lungs, resulting in a failure to inhibit viral replication and skewing the immune response toward Th2 responses (11–14). Similar lung pathology has also been observed in humans vaccinated with FI-RSV followed by RSV infection (38, 39), with the Th2-skewed cytokine profile also a hallmark of RSV vaccine-enhanced disease (40). The Th2-skewed cytokine profile is shown to be reduced only when the functions of IL-4 and IL-13, both Th2 cytokines, are blocked in FI-RSV-immunized mice (41, 42), indicating that both IL-4 and IL-13 promote the development of pulmonary eosinophilia upon RSV challenge of FI-RSV-immunized mice. High levels of Th2 cytokines, including IL-4 and IL-13, and the upregulation of genes associated with Th2 cell migration were observed in the lungs of UV-V-immunized mice, suggesting that the UV-V-specific immune response occurs in a manner similar to that of the FI-RSV vaccine. Furthermore, a few UV-V-immunized mice were unable to produce protective neutralizing antibodies and died on day 5 after challenge, showing severe inflammation, including high eosinophilia in the lungs. Interestingly, a UV-V+Alum-immunized mouse produced high titers of neutralizing antibodies in serum but died of eosinophilic pneumonia in this study. Vaccination with UV-inactivated virions of other viruses may carry a potential for dangerous clinical complications, similar to those observed for inactivated RSV vaccine. Pulmonary eosinophilia is a hallmark of an aberrant hypersensitivity response to FI-RSV (43). A recent study using eosinophil-deficient mice found that eosinophils did not contribute to RSV vaccine-enhanced pulmonary disease (44). In contrast, another study using mouse pneumonia virus, resulting in severe RSV, found that eosinophils did not promote virus clearance (45). The mechanism of vaccine-induced eosinophilia has not been determined, with no consensus as to whether eosinophils potentially contribute to protection or enhance lung immunopathology subsequent to respiratory infection.

Vaccine failure in RSV-enhanced respiratory disease was thought to be due to disruption of protective antigens by formalin. However, this lack of protection was due not to formalin-induced alterations but to low antibody avidity for protective epitopes resulting from poor TLR stimulation (18). To mimic live attenuated vaccine, mice were inoculated with HKU39849, which completely protected them from subsequent SARS-CoV infection. Moreover, these mice did not display enhanced eosinophilic infiltration in the lungs. In addition, all mock-vaccinated mice died but did not show evidence of eosinophilia. TLRs are critical to sensing invading microorganisms. Pathogen recognition by TLRs provokes the rapid activation of innate immunity, leading to effective adaptive immunity (23). Despite the protective effects of TLRs upon infection, faulty TLR signaling is increasingly implicated in the pathogenesis of allergic diseases (46, 47). We hypothesized that vaccination with UV-V was unable to generate effective immunity against SARS-CoV infection because of poor TLR stimulation, which may be enough when natural SARS-CoV infection occurs. In fact, immunizing mice with UV-V, together with the TLR agonists, poly(I·C) (a TLR3 agonist), LPS (a TLR4 agonist), and poly(U) (a TLR7 agonist), as an adjuvant, produced effective antibodies and inhibited excess eosinophilic immunopathology. The innate immunomodulatory activity in response to live and inactivated SARS-CoV is not well understood. However, mouse models of related CoV infection have suggested protective roles for TLR4 (48) and myeloid differentiation factor 88 (MyD88) (49), whereas TLR3 and TLR7 may be important for viral clearance through the production of type I IFN (50, 51).

Intranasal injection of the TLR agonist poly(I·C) into aged mice provided a high level of protection against SARS-CoV infection (51). Indeed, higher IFN-β gene expression on day 1 p.i. was seen in the lungs of UV-V+TLR-immunized mice than in those of UV-V-immunized mice. UV-V+TLR but not UV-V immunization primed the cells that expressed IFN-β after SARS-CoV infection. IFN-β was induced directly after Sendai virus infection in a murine model, leading to the expression of IFN-α genes (52). Although viral copy numbers in the lungs were similar in both groups 1 day after challenge, titers of virus differed significantly in the lung wash fluid of UV-V+TLR- and PBS-injected mice on day 3. Virus excretion into the lungs of UV-V+TLR-immunized mice on day 3 may be inhibited by IFN-β gene expression. The type I IFNs not only play an important role in the innate immune response but also enhance Th1-type responses (53). Higher IFN-β gene expression in UV-V+TLR-immunized mice may therefore contribute to the production of Th1 cytokines after viral infection.

FIG 10 Pathway analysis of the gene-to-gene networks of TLR3, TLR4, and poly(I·C) in mice immunized with UV-V after SARS-CoV challenge. Direct comparison of gene expression profiles in $CD11b^+$ cells isolated from the lungs of UV-V- and UV-V+TLR-immunized mice. (A and D) FACS analysis of enriched populations of $CD11b^+$ lung cells in UV-V-immunized (A) or UV-V+TLR-immunized (D) mice. Cells were prepared as described in Materials and Methods. (B and E) Conventional Giemsa staining of cytospins from populations of $CD11b^+$ lung cells in UV-V-immunized (B) or UV-V+TLR-immunized (E) mice (magnification, ×100). (C and F) Diagram showing the pathways of TLR3 and TLR4 signaling. Genes shown in red were upregulated, and those in green were downregulated. Several genes downstream of TLR3 and TLR4 signaling were upregulated in UV-V-immunized mice (C) compared with expression in UV-V+TLR-immunized mice (F). We overlaid gene expression data on the formed network by using Ingenuity Pathway Analysis software.

To assess the efficacy of vaccination of the mice, we demonstrated both short- and long-interval UV-V-immunization on virus challenge. The titer of neutralizing antibodies was higher after a longer period of time, and these antibodies were sufficiently protective against SARS-CoV infection. However, eosinophil infiltration in the lungs occurred in the UV-V-immunized mice.

Mice immunized with inactivated RSV plus TLR agonists produced mature antibodies following TLR stimulation, preventing enhanced respiratory disease (18). These findings suggest that TLR stimulation during immunization with UV-V plays a key role in reducing eosinophil infiltration into the lungs, with strong TLR stimulation by TLR agonists shifting the host immune response in the lungs from Th2 to Th1. In line with this, our microarray analysis showed that several genes downstream of TLR3 and TLR4 signaling were markedly upregulated in UV-V+TLR-immunized mice compared with expression in UV-V-immunized mice on day 1 after subsequent SARS-CoV infection. Furthermore, IPA analysis of $CD11b^+$ cells isolated from the lungs of UV-V+TLR-immunized mice showed upregulation of genes associated with cellular movement and maturation of antigen-presenting cells in the TLR3 and TLR4 signaling pathways. This finding indicated that UV-V+TLR but not UV-V immunization may prime effective innate immune responses against SARS-CoV infection in mice due to the intensity of TLR stimulation.

To our knowledge, this is the first study to show that vaccination with UV-inactivated whole virions plus TLR agonists provides protection against SARS-CoV infection without strong Th2 skewing; TLR stimulation reduced the high level of eosinophilic infiltration that occurred in the lungs of mice immunized with UV-V. TLR agonists are approved for human use (54), and several are currently in preclinical development for use as vaccine adjuvants (55). Further studies regarding the association of TLR stimulation with protective immunity to SARS-CoV infection, the indication that eosinophils contribute to the negative sequelae of disease, and the mechanisms of eosinophil recruitment to lung tissue are required.

ACKNOWLEDGMENTS

This work was supported by a Grant-in Aid for Young Scientists (B), no. 22790444, from the Japan Society for the Promotion of Science and Grants-in Aid for research on emerging and reemerging infectious diseases, H23-Shinko-Ippan-007 and H25-Shinko-Wakate-004, from the Ministry of Health, Labor, and Welfare, Japan.

We thank our colleagues at the institute, especially Ayako Harashima and Mihoko Fujino, for their technical assistance and Shin-ichi Tamura for valuable discussions.

REFERENCES

1. Drosten C, Gunther S, Preiser W, van der Werf S, Brodt HR, Becker S, Rabenau H, Panning M, Kolesnikova L, Fouchier RA, Berger A, Burguiere AM, Cinatl J, Eickmann M, Escriou N, Grywna K, Kramme S, Manuguerra JC, Muller S, Rickerts V, Sturmer M, Vieth S, Klenk HD, Osterhaus AD, Schmitz H, Doerr HW. 2003. Identification of a novel coronavirus in patients with severe acute respiratory syndrome. N. Engl. J. Med. 348:1967–1976. http://dx.doi.org/10.1056/NEJMoa030747.
2. Ksiazek TG, Erdman D, Goldsmith CS, Zaki SR, Peret T, Emery S, Tong S, Urbani C, Comer JA, Lim W, Rollin PE, Dowell SF, Ling AE, Humphrey CD, Shieh WJ, Guarner J, Paddock CD, Rota P, Fields B, DeRisi J, Yang JY, Cox N, Hughes JM, LeDuc JW, Bellini WJ, Anderson LJ. 2003. A novel coronavirus associated with severe acute respiratory syndrome. N. Engl. J. Med. 348:1953–1966. http://dx.doi.org/10.1056/NEJMoa030781.
3. Peiris JSM, Lai ST, Poon LLM, Guan Y, Yam LYC, Lim W, Nicholls J, Yee WKS, Yan WW, Cheung MT, Cheng VCC, Chan KH, Tsang DNC, Yung RWH, Ng TK, Yuen KY. 2003. Coronavirus as a possible cause of severe acute respiratory syndrome. Lancet 361:1319–1325. http://dx.doi.org/10.1016/S0140-6736(03)13077-2.
4. Rota PA, Oberste MS, Monroe SS, Nix WA, Campagnoli R, Icenogle JP, Penaranda S, Bankamp B, Maher K, Chen MH, Tong S, Tamin A, Lowe L, Frace M, DeRisi JL, Chen Q, Wang D, Erdman DD, Peret TC, Burns C, Ksiazek TG, Rollin PE, Sanchez A, Liffick S, Holloway B, Limor J, McCaustland K, Olsen-Rasmussen M, Fouchier R, Gunther S, Osterhaus AD, Drosten C, Pallansch MA, Anderson LJ, Bellini WJ. 2003. Characterization of a novel coronavirus associated with severe acute respiratory syndrome. Science 300:1394–1399. http://dx.doi.org/10.1126/science.1085952.
5. He Y, Zhou Y, Siddiqui P, Jiang S. 2004. Inactivated SARS-CoV vaccine elicits high titers of spike protein-specific antibodies that block receptor binding and virus entry. Biochem. Biophys. Res. Commun. 325:445–452. http://dx.doi.org/10.1016/j.bbrc.2004.10.052.
6. Takasuka N, Fujii H, Takahashi Y, Kasai M, Morikawa S, Itamura S, Ishii K, Sakaguchi M, Ohnishi K, Ohshima M, Hashimoto S, Odagiri T, Tashiro M, Yoshikura H, Takemori T, Tsunetsugu-Yokota Y. 2004. A subcutaneously injected UV-inactivated SARS coronavirus vaccine elicits systemic humoral immunity in mice. Int. Immunol. 16:1423–1430. http://dx.doi.org/10.1093/intimm/dxh143.
7. Tang L, Zhu Q, Qin E, Yu M, Ding Z, Shi H, Cheng X, Wang C, Chang G, Zhu Q, Fang F, Chang H, Li S, Zhang X, Chen X, Yu J, Wang J, Chen Z. 2004. Inactivated SARS-CoV vaccine prepared from whole virus induces a high level of neutralizing antibodies in BALB/c mice. DNA Cell Biol. 23:391–394. http://dx.doi.org/10.1089/104454904323145272.
8. Xiong S, Wang YF, Zhang MY, Liu XJ, Zhang CH, Liu SS, Qian CW, Li JX, Lu JH, Wan ZY, Zheng HY, Yan XG, Meng MJ, Fan JL. 2004. Immunogenicity of SARS inactivated vaccine in BALB/c mice. Immunol. Lett. 95:139–143. http://dx.doi.org/10.1016/j.imlet.2004.06.014.
9. Qu D, Zheng B, Yao X, Guan Y, Yuan ZH, Zhong NS, Lu LW, Xie JP, Wen YM. 2005. Intranasal immunization with inactivated SARS-CoV (SARS-associated coronavirus) induced local and serum antibodies in mice. Vaccine 23:924–931. http://dx.doi.org/10.1016/j.vaccine.2004.07.031.
10. Zhang CH, Lu JH, Wang YF, Zheng HY, Xiong S, Zhang MY, Liu XJ, Li JX, Wan ZY, Yan XG, Qi SY, Cui Z, Zhang B. 2005. Immune responses in Balb/c mice induced by a candidate SARS-CoV inactivated vaccine prepared from F69 strain. Vaccine 23:3196–3201. http://dx.doi.org/10.1016/j.vaccine.2004.11.073.
11. Deming D, Sheahan T, Heise M, Yount B, Davis N, Sims A, Suthar M, Harkema J, Whitmore A, Pickles R, West A, Donaldson E, Curtis K, Johnston R, Baric R. 2006. Vaccine efficacy in senescent mice challenged with recombinant SARS-CoV bearing epidemic and zoonotic spike variants. PLoS Med. 3:e525. http://dx.doi.org/10.1371/journal.pmed.0030525.
12. Yasui F, Kai C, Kitabatake M, Inoue S, Yoneda M, Yokochi S, Kase R, Sekiguchi S, Morita K, Hishima T, Suzuki H, Karamatsu K, Yasutomi Y, Shida H, Kidokoro M, Mizuno K, Matsushima K, Kohara M. 2008. Prior immunization with severe acute respiratory syndrome (SARS)-associated coronavirus (SARS-CoV) nucleocapsid protein causes severe pneumonia in mice infected with SARS-CoV. J. Immunol. 181:6337–6348. http://dx.doi.org/10.4049/jimmunol.181.9.6337.
13. Bolles M, Deming D, Long K, Agnihothram S, Whitmore A, Ferris M, Funkhouser W, Gralinski L, Totura A, Heise M, Baric RS. 2011. A double-inactivated severe acute respiratory syndrome coronavirus vaccine provides incomplete protection in mice and induces increased eosinophilic proinflammatory pulmonary response upon challenge. J. Virol. 85:12201–12215. http://dx.doi.org/10.1128/JVI.06048-11.
14. Tseng CT, Sbrana E, Iwata-Yoshikawa N, Newman PC, Garron T, Atmar RL, Peters CJ, Couch RB. 2012. Immunization with SARS coronavirus vaccines leads to pulmonary immunopathology on challenge with the SARS virus. PLoS One 7:e35421. http://dx.doi.org/10.1371/journal.pone.0035421.
15. Neuman BW, Adair BD, Yoshioka C, Quispe JD, Orca G, Kuhn P, Milligan RA, Yeager M, Buchmeier MJ. 2006. Supramolecular architecture of severe acute respiratory syndrome coronavirus revealed by electron cryomicroscopy. J. Virol. 80:7918–7928. http://dx.doi.org/10.1128/JVI.00645-06.
16. Kim HW, Canchola JG, Brandt CD, Pyles G, Chanock RM, Jensen K, Parrott RH. 1969. Respiratory syncytial virus disease in infants despite prior administration of antigenic inactivated vaccine. Am. J. Epidemiol. 89:422–434.

17. **Olson MR, Varga SM.** 2008. Pulmonary immunity and immunopathology: lessons from respiratory syncytial virus. Expert Rev. Vaccines **7**:1239–1255. http://dx.doi.org/10.1586/14760584.7.8.1239.
18. **Delgado MF, Coviello S, Monsalvo AC, Melendi GA, Hernandez JZ, Batalle JP, Diaz L, Trento A, Chang HY, Mitzner W, Ravetch J, Melero JA, Irusta PM, Polack FP.** 2009. Lack of antibody affinity maturation due to poor Toll-like receptor stimulation leads to enhanced respiratory syncytial virus disease. Nat. Med. **15**:34–41. http://dx.doi.org/10.1038/nm.1894.
19. **Nagata N, Iwata N, Hasegawa H, Fukushi S, Harashima A, Sato Y, Saijo M, Taguchi F, Morikawa S, Sata T.** 2008. Mouse-passaged severe acute respiratory syndrome-associated coronavirus leads to lethal pulmonary edema and diffuse alveolar damage in adult but not young mice. Am. J. Pathol. **172**:1625–1637. http://dx.doi.org/10.2353/ajpath.2008.071060.
20. **Nagata N, Iwata N, Hasegawa H, Sato Y, Morikawa S, Saijo M, Itamura S, Saito T, Ami Y, Odagiri T, Tashiro M, Sata T.** 2007. Pathology and virus dispersion in cynomolgus monkeys experimentally infected with severe acute respiratory syndrome coronavirus via different inoculation routes. Int. J. Exp. Pathol. **88**:403–414. http://dx.doi.org/10.1111/j.1365-2613.2007.00567.x.
21. **Zhang X, Goncalves R, Mosser DM.** 2008. The isolation and characterization of murine macrophages. Curr. Protoc. Immunol. **83**:14.1–14.1.14. http://dx.doi.org/10.1002/0471142735.im1401s83.
22. **Sugiura N, Uda A, Inoue S, Kojima D, Hamamoto N, Kaku Y, Okutani A, Noguchi A, Park CH, Yamada A.** 2011. Gene expression analysis of host innate immune responses in the central nervous system following lethal CVS-11 infection in mice. Jpn. J. Infect. Dis. **64**:463–472.
23. **Kaisho T, Akira S.** 2002. Toll-like receptors as adjuvant receptors. Biochim. Biophys. Acta **1589**:1–13. http://dx.doi.org/10.1016/S0167-4889(01)00182-3.
24. **Pashine A, Valiante NM, Ulmer JB.** 2005. Targeting the innate immune response with improved vaccine adjuvants. Nat. Med. **11**:S63–S68. http://dx.doi.org/10.1038/nm1210.
25. **O'Neill LA, Bowie AG.** 2007. The family of five: TIR-domain-containing adaptors in Toll-like receptor signalling. Nat. Rev. Immunol. **7**:353–364. http://dx.doi.org/10.1038/nri2079.
26. **O'Mahony DS, Pham U, Iyer R, Hawn TR, Liles WC.** 2008. Differential constitutive and cytokine-modulated expression of human Toll-like receptors in primary neutrophils, monocytes, and macrophages. Int. J. Med. Sci. **5**:1–8. http://dx.doi.org/10.7150/ijms.5.1.
27. **Applequist SE, Wallin RP, Ljunggren HG.** 2002. Variable expression of Toll-like receptor in murine innate and adaptive immune cell lines. Int. Immunol. **14**:1065–1074. http://dx.doi.org/10.1093/intimm/dxf069.
28. **Roper RL, Rehm KE.** 2009. SARS vaccines: where are we? Expert Rev. Vaccines **8**:887–898. http://dx.doi.org/10.1586/erv.09.43.
29. **Buchholz UJ, Bukreyev A, Yang L, Lamirande EW, Murphy BR, Subbarao K, Collins PL.** 2004. Contributions of the structural proteins of severe acute respiratory syndrome coronavirus to protective immunity. Proc. Natl. Acad. Sci. U. S. A. **101**:9804–9809. http://dx.doi.org/10.1073/pnas.0403492101.
30. **Bukreyev A, Lamirande EW, Buchholz UJ, Vogel LN, Elkins WR, St Claire M, Murphy BR, Subbarao K, Collins PL.** 2004. Mucosal immunisation of African green monkeys (Cercopithecus aethiops) with an attenuated parainfluenza virus expressing the SARS coronavirus spike protein for the prevention of SARS. Lancet **363**:2122–2127. http://dx.doi.org/10.1016/S0140-6736(04)16501-X.
31. **Ishii K, Hasegawa H, Nagata N, Mizutani T, Morikawa S, Suzuki T, Taguchi F, Tashiro M, Takemori T, Miyamura T, Tsunetsugu-Yokota Y.** 2006. Induction of protective immunity against severe acute respiratory syndrome coronavirus (SARS-CoV) infection using highly attenuated recombinant vaccinia virus DIs. Virology **351**:368–380. http://dx.doi.org/10.1016/j.virol.2006.03.020.
32. **Guo JP, Petric M, Campbell W, McGeer PL.** 2004. SARS corona virus peptides recognized by antibodies in the sera of convalescent cases. Virology **324**:251–256. http://dx.doi.org/10.1016/j.virol.2004.04.017.
33. **Hanley KA.** 2011. The double-edged sword: how evolution can make or break a live-attenuated virus vaccine. Evolution **4**:635–643. http://dx.doi.org/10.1007/s12052-011-0365-y.
34. **DeDiego ML, Alvarez E, Almazan F, Rejas MT, Lamirande E, Roberts A, Shieh WJ, Zaki SR, Subbarao K, Enjuanes L.** 2007. A severe acute respiratory syndrome coronavirus that lacks the E gene is attenuated in vitro and in vivo. J. Virol. **81**:1701–1713. http://dx.doi.org/10.1128/JVI.01467-06.
35. **Dediego ML, Pewe L, Alvarez E, Rejas MT, Perlman S, Enjuanes L.** 2008. Pathogenicity of severe acute respiratory coronavirus deletion mutants in hACE-2 transgenic mice. Virology **376**:379–389. http://dx.doi.org/10.1016/j.virol.2008.03.005.
36. **Lamirande EW, DeDiego ML, Roberts A, Jackson JP, Alvarez E, Sheahan T, Shieh WJ, Zaki SR, Baric R, Enjuanes L, Subbarao K.** 2008. A live attenuated severe acute respiratory syndrome coronavirus is immunogenic and efficacious in golden Syrian hamsters. J. Virol. **82**:7721–7724. http://dx.doi.org/10.1128/JVI.00304-08.
37. **Tsunetsugu-Yokota Y.** 2008. Large-scale preparation of UV-inactivated SARS coronavirus virions for vaccine antigen. Methods Mol. Biol. **454**:119–126. http://dx.doi.org/10.1007/978-1-59745-181-9_11.
38. **Hancock GE, Speelman DJ, Heers K, Bortell E, Smith J, Cosco C.** 1996. Generation of atypical pulmonary inflammatory responses in BALB/c mice after immunization with the native attachment (G) glycoprotein of respiratory syncytial virus. J. Virol. **70**:7783–7791.
39. **De Swart RL, Kuiken T, Timmerman HH, van Amerongen G, Van Den Hoogen BG, Vos HW, Neijens HJ, Andeweg AC, Osterhaus AD.** 2002. Immunization of macaques with formalin-inactivated respiratory syncytial virus (RSV) induces interleukin-13-associated hypersensitivity to subsequent RSV infection. J. Virol. **76**:11561–11569. http://dx.doi.org/10.1128/JVI.76.22.11561-11569.2002.
40. **Johnson TR, Varga SM, Braciale TJ, Graham BS.** 2004. Vbeta14(+) T cells mediate the vaccine-enhanced disease induced by immunization with respiratory syncytial virus (RSV) G glycoprotein but not with formalin-inactivated RSV. J. Virol. **78**:8753–8760. http://dx.doi.org/10.1128/JVI.78.16.8753-8760.2004.
41. **Johnson TR, Graham BS.** 1999. Secreted respiratory syncytial virus G glycoprotein induces interleukin-5 (IL-5), IL-13, and eosinophilia by an IL-4-independent mechanism. J. Virol. **73**:8485–8495.
42. **Johnson TR, Parker RA, Johnson JE, Graham BS.** 2003. IL-13 is sufficient for respiratory syncytial virus G glycoprotein-induced eosinophilia after respiratory syncytial virus challenge. J. Immunol. **170**:2037–2045. http://dx.doi.org/10.4049/jimmunol.170.4.2037.
43. **Rosenberg HF, Dyer KD, Domachowske JB.** 2009. Respiratory viruses and eosinophils: exploring the connections. Antiviral Res. **83**:1–9. http://dx.doi.org/10.1016/j.antiviral.2009.04.005.
44. **Castilow EM, Legge KL, Varga SM.** 2008. Cutting edge: eosinophils do not contribute to respiratory syncytial virus vaccine-enhanced disease. J. Immunol. **181**:6692–6696. http://dx.doi.org/10.4049/jimmunol.181.10.6692.
45. **Percopo CM, Qiu Z, Phipps S, Foster PS, Domachowske JB, Rosenberg HF.** 2009. Pulmonary eosinophils and their role in immunopathologic responses to formalin-inactivated pneumonia virus of mice. J. Immunol. **183**:604–612. http://dx.doi.org/10.4049/jimmunol.0802270.
46. **Horner AA, Raz E.** 2003. Do microbes influence the pathogenesis of allergic diseases? Building the case for Toll-like receptor ligands. Curr. Opin. Immunol. **15**:614–619. http://dx.doi.org/10.1016/j.coi.2003.09.021.
47. **Vercelli D.** 2006. Mechanisms of the hygiene hypothesis—molecular and otherwise. Curr. Opin. Immunol. **18**:733–737. http://dx.doi.org/10.1016/j.coi.2006.09.002.
48. **Khanolkar A, Hartwig SM, Haag BA, Meyerholz DK, Harty JT, Varga SM.** 2009. Toll-like receptor 4 deficiency increases disease and mortality after mouse hepatitis virus type 1 infection of susceptible C3H mice. J. Virol. **83**:8946–8956. http://dx.doi.org/10.1128/JVI.01857-08.
49. **Sheahan T, Morrison TE, Funkhouser W, Uematsu S, Akira S, Baric RS, Heise MT.** 2008. MyD88 is required for protection from lethal infection with a mouse-adapted SARS-CoV. PLoS Pathog. **4**:e1000240. http://dx.doi.org/10.1371/journal.ppat.1000240.
50. **Cervantes-Barragan L, Zust R, Weber F, Spiegel M, Lang KS, Akira S, Thiel V, Ludewig B.** 2007. Control of coronavirus infection through plasmacytoid dendritic-cell-derived type I interferon. Blood **109**:1131–1137. http://dx.doi.org/10.1182/blood-2006-05-023770.
51. **Zhao J, Wohlford-Lenane C, Zhao J, Fleming E, Lane TE, McCray PB, Jr, Perlman S.** 2012. Intranasal treatment with poly(I·C) protects aged mice from lethal respiratory virus infections. J. Virol. **86**:11416–11424. http://dx.doi.org/10.1128/JVI.01410-12.
52. **Erlandsson L, Blumenthal R, Eloranta ML, Engel H, Alm G, Weiss S, Leanderson T.** 1998. Interferon-beta is required for interferon-alpha production in mouse fibroblasts. Curr. Biol. **8**:223–226. http://dx.doi.org/10.1016/S0960-9822(98)70086-7.
53. **Biron CA.** 1998. Role of early cytokines, including alpha and beta interferons (IFN-alpha/beta), in innate and adaptive immune responses to

viral infections. Semin. Immunol. **10**:383–390. http://dx.doi.org/10.1006/smim.1998.0138.

54. **Kanzler H, Barrat FJ, Hessel EM, Coffman RL.** 2007. Therapeutic targeting of innate immunity with Toll-like receptor agonists and antagonists. Nat. Med. **13**:552–559. http://dx.doi.org/10.1038/nm1589.
55. **Horscroft NJ, Pryde DC, Bright H.** 2012. Antiviral applications of Toll-like receptor agonists. J. Antimicrob. Chemother. **67**:789–801. http://dx.doi.org/10.1093/jac/dkr588.
56. **Keyaerts E, Vijgen L, Maes P, Duson G, Neyts J, Van Ranst M.** 2006. Viral load quantitation of SARS-coronavirus RNA using a one-step real-time RT-PCR. Int. J. Infect. Dis. **10**:32–37. http://dx.doi.org/10.1016/j.ijid.2005.02.003.